Chapter 8

RESULTS

This chapter presents the results and interpretation of the analysis performed in **??**. Once a theory has been described (**??**), the data collected (**????**) and reconstructed (**??**), analyzed and with systematics accounted for (**??**), the search regions can be applied to data, compared to monte-carlo signal and background models, and hypothesis testing performed to determine if new physics has been found.

Once the monte-carlo is normalized using a data-driven method (**??**), the results need to first be validated in a background-only fit described in section 8.2.1. If there are no significant deviations in the modeling of data in the validation regions, **unblinding**, section 8.2.2, can happen where data is allowed to fill in the signal regions. Finally, as there is no significant excess observed in the cut-and-count analysis, exclusion limits are set using the CLs method in section 8.3. To wrap up the interpretation, truth acceptances and signal region selection efficiences are described in section 8.4 for theorists and users who wish to reinterpret the results of the analysis.

8.1 General Likelihood

Here, I try to use consistent notation so that $n_{\text{subscript}}$ refers to observed events, a number corresponding to data yields in the given region, while $s_{\text{subscript}}$ and $b_{\text{subscript}}$ refer to predicted yields for signal and background, respectively, corresponding to yields from monte-carlo simulation in the given region. The exception is for n_{pred} which refers to the total predicted yield of backgrounds and signal.

$$L(\boldsymbol{n}, \boldsymbol{\theta^0}|\mu_{\text{sig}}, \boldsymbol{b}, \boldsymbol{\theta}) = \underbrace{P(n_S|\lambda_S(\mu_{\text{sig}}, \boldsymbol{b}, \boldsymbol{\theta}))}_{P_{\text{SR}}} \times \underbrace{P(n_{t\bar{t}}|\lambda_{t\bar{t}}(\mu_{\text{sig}}, \boldsymbol{b}, \boldsymbol{\theta}))}_{P_{\text{CR}}} \times \underbrace{C_{\text{syst}}(\boldsymbol{\theta^0}, \boldsymbol{\theta})}_{C_{\text{syst}}} \tag{8.1}$$

The general likelihood[1] L (eq. (8.1)) fit of analyses is a product of the Poissonian distributions of event yields in the signal regions and control regions of interest [1, 2]. As the analysis strategy was designed to minimize the signal contamination in the control region, the normalization $\mu_{t\bar{t}}$ will depend on the amount of signal, μ_{sig}. Similarly, because the signal regions are designed to maximize Supersymmetry (SUSY) discovery, this will depend on the amount of background present in the signal regions. This likelihood is used to perform hypothesis testing on the predicted number of events in the signal region described with monte-carlo simulation, n_{pred}, compared to the observed number of events seen by data. Equation (8.2) describes the number of predicted events n_{pred} as a function of number of predicted signal events s, number of predicted $t\bar{t}$ events $b_{t\bar{t}}$ scaled by the transfer factor $\mu_{t\bar{t}}$, and the predicted yields of other backgrounds $\boldsymbol{b}_{\text{other}}$. μ_{sig} is a binary parameter with $\mu_{\text{sig}} = 0$ for a background-only fit (no signal models are used) and $\mu_{\text{sig}} = 1$ for a total fit for discovery or setting exclusion limits. The likelihood describes the the normalization factors for background processes such as $t\bar{t}$ (using data-driven techniques) as well as the **nuisance parameters**, $\boldsymbol{\theta}$, that parameterize the systematic uncertainties, $\boldsymbol{\theta} \sim (\theta_0, \theta_1, \ldots, \theta_m) \equiv \theta_i$ for the m systematic uncertainties. Each θ_i is a nuisance parameter that continuously interpolates from nominal variation to a systematic variable, such as from $\theta_i = \theta^0 \equiv 0 \mapsto \pm 1$ for $\pm 1\sigma$ variations[2]. Systematics can kill an experimental observation if they are not under control. In the limit of large numbers, the significance of an observation is $S/\sqrt{B}$. In the presence of systematics, this significance is smaller. For example, if there is a systematic uncertainty

[1] Also referred to as the "extended maximum likelihood fit".

[2] One standard deviation.

θ_B on the background, the significance becomes something like $S/\sqrt{B(1+\theta_B^2 B)} \to S/B\theta_B$ in the limit of large background, and so a large systematic uncertainty can make it difficult if not impossible to achieve a significant observation. And finally, λ_i are part of Poissonian expectations that are functions of the background predictions and the systematics, the normalization factor for background processes, and μ_{sig} [2] as shown in eq. (8.3).

$$n_{\text{pred}} = \mu_{\text{sig}} s + \underbrace{\mu_{t\bar{t}} b_{t\bar{t}} + \boldsymbol{b}_{\text{other}}}_{\boldsymbol{b}} \tag{8.2}$$

$$P(k|\lambda) = \frac{\lambda^k e^{-\lambda}}{k!} \tag{8.3}$$

Systematic uncertainties are included in this likelihood through the probability density function C_{syst} which describes the variations of $\boldsymbol{\theta}$ around $\boldsymbol{\theta^0}$. Changes in the nuisance parameters are described by λ_S and λ_i, the functions that predict signal and background. If each systematic is described by a Gaussian with $\sigma = 1$, the probability density function C_{syst} can be written as in eq. (8.4)

$$C_{\text{syst}}(\boldsymbol{\theta^0}, \boldsymbol{\theta}) = \prod_{\text{all systematics}} \frac{1}{\sqrt{2\pi}} e^{-\frac{1}{2}(\theta_i^0 - \theta_i)^2}. \tag{8.4}$$

8.2 Background-only Fit

8.2.1 Validation

In order to verify that our normalization in **??** is well-modeled, validation regions are defined in a way to minimize the contribution from signal while remaining orthogonal to control re-

gions to suppress any effects of cross-correlation. This procedure is done using something called a **background-only fit** [1] which propagates the estimate of the $t\bar{t}$ normalization factor, $\mu_{t\bar{t}}$, to the corresponding validation and signal regions, allowing us to predict the background event yields in the validation regions and signal regions. As the background-only fit only uses the control regions in the fit, this allows for external groups to use the background-only fit results to perform hypothesis testing on an entirely different untested signal model not studied by the current analysis. This prcoedure is known as **reinterpretation** [3].

Figure 8.1 shows the results of the background-only fit to the control regions, extrapolated to the validation regions for the cut-and-count analysis. The number of events predicted by the background-only fit is compared to data in the upper pannel. The pull, χ, (eq. (8.5a)), defined by the difference between the observed number of events, n_{obs}, and the predicted background yield, n_{pred}, divided by the total uncertainty, σ_{tot} is shown for each region in the lower panel. The total uncertainty is the total systematic uncertainty on the background prediction, σ_{pred} (described in **??**), added in quadrature to the Poissonian variation on the expected number of background events, $\sigma_{\text{stat, exp}}$. On average, if the pulls for all validation regions are negative (positive), the data is overestimated (underestimated) and the background model needs to be corrected.

$$\chi \equiv \text{pull} = \frac{n_{\text{obs}} - n_{\text{pred}}}{\sigma_{\text{tot}}} \tag{8.5a}$$

$$\sigma_{\text{tot}} = \sigma_{\text{pred}} \otimes \sigma_{\text{stat, exp}} \tag{8.5b}$$

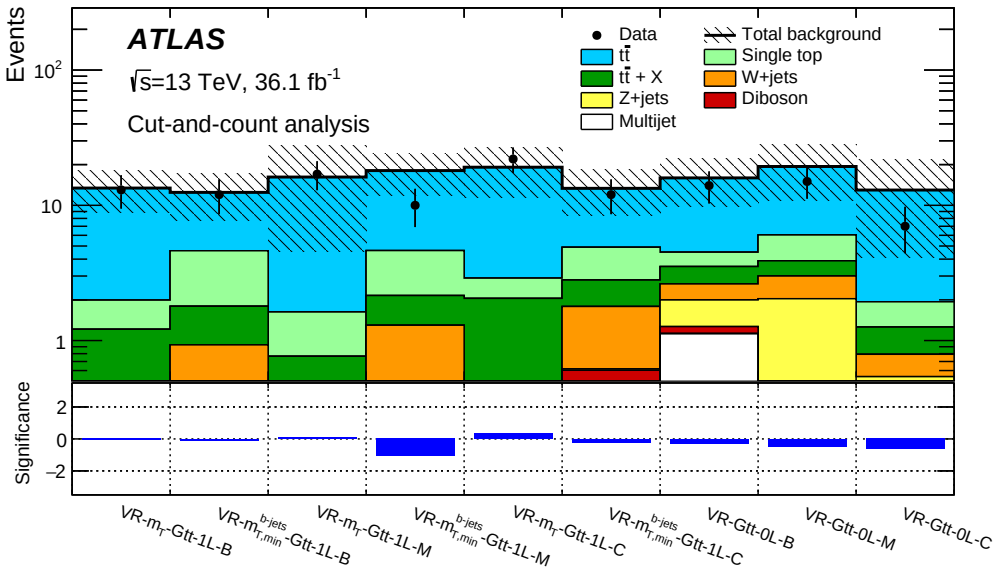

Figure 8.1: Results of the background-only fit extrapolated to the validation regions of the cut-and-count analysis. The $t\bar{t}$ normalization, $\mu_{t\bar{t}}$, is obtained from the fit to the control regions shown in **??**. The upper panel shows the observed number of events and the predicted background yield. All uncertainties are included in the uncertainty band. The background category $t\bar{t}$ +X includes $t\bar{t}$ +W/Z, $t\bar{t}$ +H and $t\bar{t}$ $t\bar{t}$ events. The lower panel shows the pulls in each validation region.

8.2.2 Unblinding

As seen in section 8.2.1, none of the pulls exceed 2σ[3] which indicates no significant mis-modeling. Given the successful validation, one proceeds to look at the background-only fit in the signal regions, unblinded, which means to include observations (data) as well. The analysis is initially blinded to minimize bias towards region definitions, and through a formal procedure within ATLAS, an analysis can go through approval to unblind. The event yields in the unblinded signal regions for the cut-and-count analysis is shown in fig. 8.2 where the pull (eq. (8.5a)) is shown for each region in the lower panel. The background is dominated by $t\bar{t}$ in all signal regions. For 0-lepton regions, the subdominant background is $Z(\to \nu\nu)$+jets and $W(\to \ell\nu)$+jets[4]. For the 1-lepton regions, the subdominant background is single-top, $t\bar{t}W$, and $t\bar{t}Z$. No significant excess is found above the predicted background. Table 8.1 shows the observed and predicted number of events from the background-only fit in the Gtt 0-lepton and 1-lepton regions for the cut-and-count analysis. The central value of the fitted background is, in general, larger than the MC-only prediction. This is primarily due to an underestimation of the cross-section of $t\bar{t}+ \geq 1b$ and $t\bar{t} \geq 1c$ [4].

8.3 Limits

Since there is no significant excess over the expected background from Standard Model processes, the data is included in an exclusion fit to derive one-sided upper limits at 95% Confidence Level (CL). The limits are calculated using the CL_s[5] prescription [6]. In particular the CL_s method is derived from the probability density functions of $-2\ln(Q)$ with Q

[3]Remember, 95% CL.

[4]Because these are subdominant in the 0-lepton regions, the lepton is either an unidentified electron, muon, or a hadronically-decaying τ lepton.

[5]This has an unfortunate name.

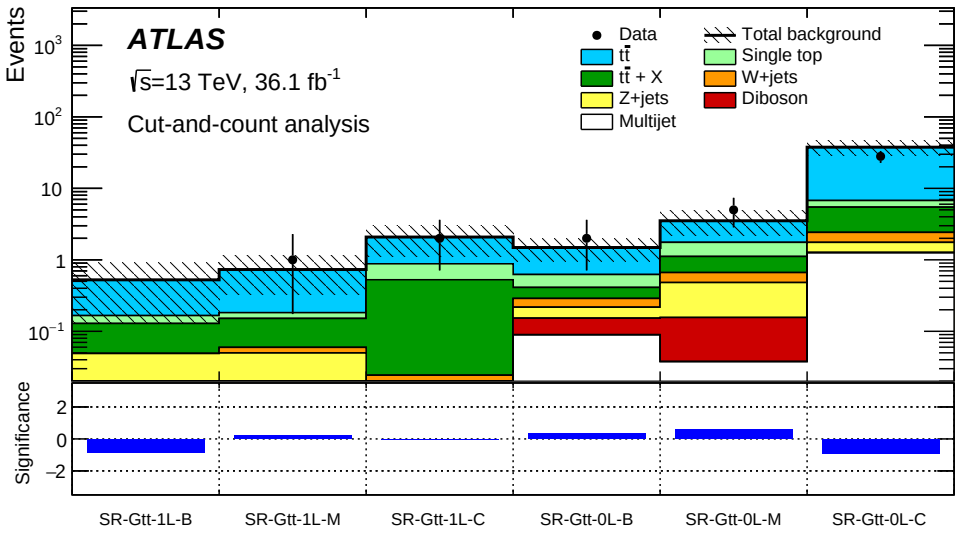

Figure 8.2: Results of the background-only fit extrapolated to the unblinded signal regions of the cut-and-count analysis. The $t\bar{t}$ normalization, $\mu_{t\bar{t}}$, is obtained from the fit to the control regions shown in **??**. The data in the signal regions are not included in the fit. The upper panel shows the observed number of events and the predicted background yield. All uncertainties are included in the uncertainty band. The background category $t\bar{t}$ +X includes $t\bar{t}$ +W/Z, $t\bar{t}$ +H and $t\bar{t}$ $t\bar{t}$ events. The lower panel shows the pulls in each signal region.

	SR-Gtt-1L		
Targeted kinematics	B	M	C
Observed events	0	1	2
Fitted background	0.5 ± 0.4	0.7 ± 0.4	2.1 ± 1.0
$t\bar{t}$	0.4 ± 0.4	0.5 ± 0.4	1.2 ± 0.8
Single-top	0.04 ± 0.05	0.03 ± 0.06	0.35 ± 0.28
$t\bar{t}+X$	0.08 ± 0.05	0.09 ± 0.06	0.50 ± 0.28
Z+jets	0.049 ± 0.023	0.050 ± 0.023	< 0.01
W+jets	< 0.01	< 0.01	0.024 ± 0.026
Diboson	< 0.01	< 0.01	< 0.01
MC-only background	0.43	0.45	1.9

	SR-Gtt-0L		
Targeted kinematics	B	M	C
Observed events	2	5	28
Fitted background	1.5 ± 0.5	3.5 ± 1.3	38 ± 8
$t\bar{t}$	0.9 ± 0.4	1.8 ± 0.7	31 ± 8
Single-top	0.21 ± 0.14	0.6 ± 0.4	1.3 ± 1.1
$t\bar{t}+X$	0.12 ± 0.07	0.45 ± 0.25	3.0 ± 1.6
Z+jets	0.06 ± 0.10	0.3 ± 0.9	0.49 ± 0.31
W+jets	0.07 ± 0.06	0.18 ± 0.15	0.67 ± 0.22
Diboson	0.06 ± 0.07	0.12 ± 0.07	< 0.01
Multijet	0.09 ± 0.11	0.04 ± 0.05	1.3 ± 2.1
MC-only background	1.3	3.3	23

Table 8.1: Results of the background-only fit extrapolated to the Gtt zero and one lepton signal regions in the cut-and-count analysis, for the total background prediction and breakdown of the main background sources. The uncertainties shown include all systematic uncertainties. The data in the signal regions are not included in the fit. The background category $t\bar{t}+X$ includes $t\bar{t}W/Z$, $t\bar{t}H$, $t\bar{t}t\bar{t}$ events. The row "MC-only background" provides the total background prediction when the $t\bar{t}$ normalization is obtained from a theoretical calculation [5].

being the ratio of likelihoods (eq. (8.1)) for the two hypotheses of interests for the exclusion test [7] in eq. (8.6). As a consequence of the Neyman-Pearson lemma [8], if H_0 is the null hypothesis (background-only) and H_1 is the alternatate hypothesis (signal + background), then the most powerful statistic one can construct is the likelihood ratio in eq. (8.6). Both hypotheses can be parameterized by μ_{sig} such as $h = \mu_{\text{sig}}s + b$ where a background-only hypothesis corresponds to $\mu_{\text{sig}} = 0$, and a signal+background hypothesis corresponds to $\mu_{\text{sig}} = 1$.

$$Q \equiv \frac{L(s+b)}{L(b)}. \tag{8.6}$$

To illustrate how the CL_s method works, I refer to fig. 8.3 where blue corresponds to a background and red corresponds to the background+signal, both are poisson distributed with the given means. In the context of this example, a likelihood for observing n_{obs} events in data with a hypothesis is defined as $p(n_{\text{obs}}|\text{hypothesis})$. $p(10|b) = 0.014$ (shaded blue). A p-value, p_b, corresponding to this is the probability of a future measurement with $n \geq n_{\text{obs}}$ for the background-only hypothesis ($\mu_{\text{sig}} = 0$) used to quantify a **discovery**, an excess of events over the background expectation. For the signal+background hypothesis $p(10|s+b) = 0.583$ (shaded red). Similarly, a p-value, p_{s+b}, corresponding to this is the probability of a future measurement with $n \leq n_{\text{obs}}$ for the signal+background hypothesis[6]. These are formally summarized in eq. (8.7a).

$$p_{s+b} = \int_{-\infty}^{N_{\text{obs}}} \text{Poisson}(q(\mu_{\text{sig}} = 1))\text{d}N \tag{8.7a}$$

$$p_b = \int_{N_{\text{obs}}}^{\infty} \text{Poisson}(q(\mu_{\text{sig}} = 0))\text{d}N \tag{8.7b}$$

[6]Note the inverted integral here!

The convention in ATLAS is to then define the upper limit as the point at which $p_{\mathrm{s+b}} = 0.05$. Signal models[7] with $p_{\mathrm{s+b}} > 0.05$ are excluded at the 95% CL while signal models with $p_{\mathrm{s+b}} < 0.05$ are not excluded. This definition of $p_{\mathrm{s+b}}$ is reasonable for setting limits, given the assumption that observed data is at least consistent with background. However, if observed data has a downward fluctuation with respect to the background expectation, then one can exclude a signal model with $\mu_{\mathrm{sig}} = 0$, as well as all signal models for $0 < \mu_{\mathrm{sig}} < 1$! Going back to fig. 8.3, but instead setting $n_{\mathrm{obs}} = 1$ (below background), one will find that $p_{\mathrm{s+b}} = 0.04$ for $\mu_{\mathrm{sig}} \sim 0$ which produces artificially strong limits at 95% CL!

In order to place limits on new physics and solve the problem of data with a downward fluctuation with respect to data, a new quantifier, called CL_s, incorporates p_{s+b} but uses p_b to regulate the behavior of n_{pred} compared to predicted b as shown in eq. (8.8)

$$\mathrm{CL}_s = \frac{p_{s+b}}{1 - p_b} = \frac{\mathrm{CL}_{s+b}}{\mathrm{CL}_b}. \tag{8.8}$$

The CL_s value is used to set exclusion limits on specific models [7]. Equation (8.6) is a simplified form of this likelihood. The LHC standard is the profile likelihood from the Neyman-Pearson lemma [8] in eq. (8.9) where $\hat{\mu}, \hat{\theta}$ are computed to maximize the likelihood function, $\hat{\hat{\theta}}$ is calculated to maximize the likelihood function for the particular μ. This new definition allows us to consider the hypothesis testing as comparing the compatibility of data with signal and background with respect to just background alone.

$$q(\mu_{\mathrm{sig}}) = -2 \ln \left(\frac{L(\mu, \hat{\hat{\theta}})}{L(\hat{\mu}, \hat{\theta})} \right). \tag{8.9}$$

[7] One can imagine, for the provided example here, signal models as being more poisson distributions with $\mu > 10$, such as for $\mu = 15, 20, \ldots$. As these get further and further away from the observed value, it becomes a matter of identifying which value of μ (by interpolation) is the limit at which you cannot exclude the distribution anymore; e.g. to fail to reject the null hypothesis.

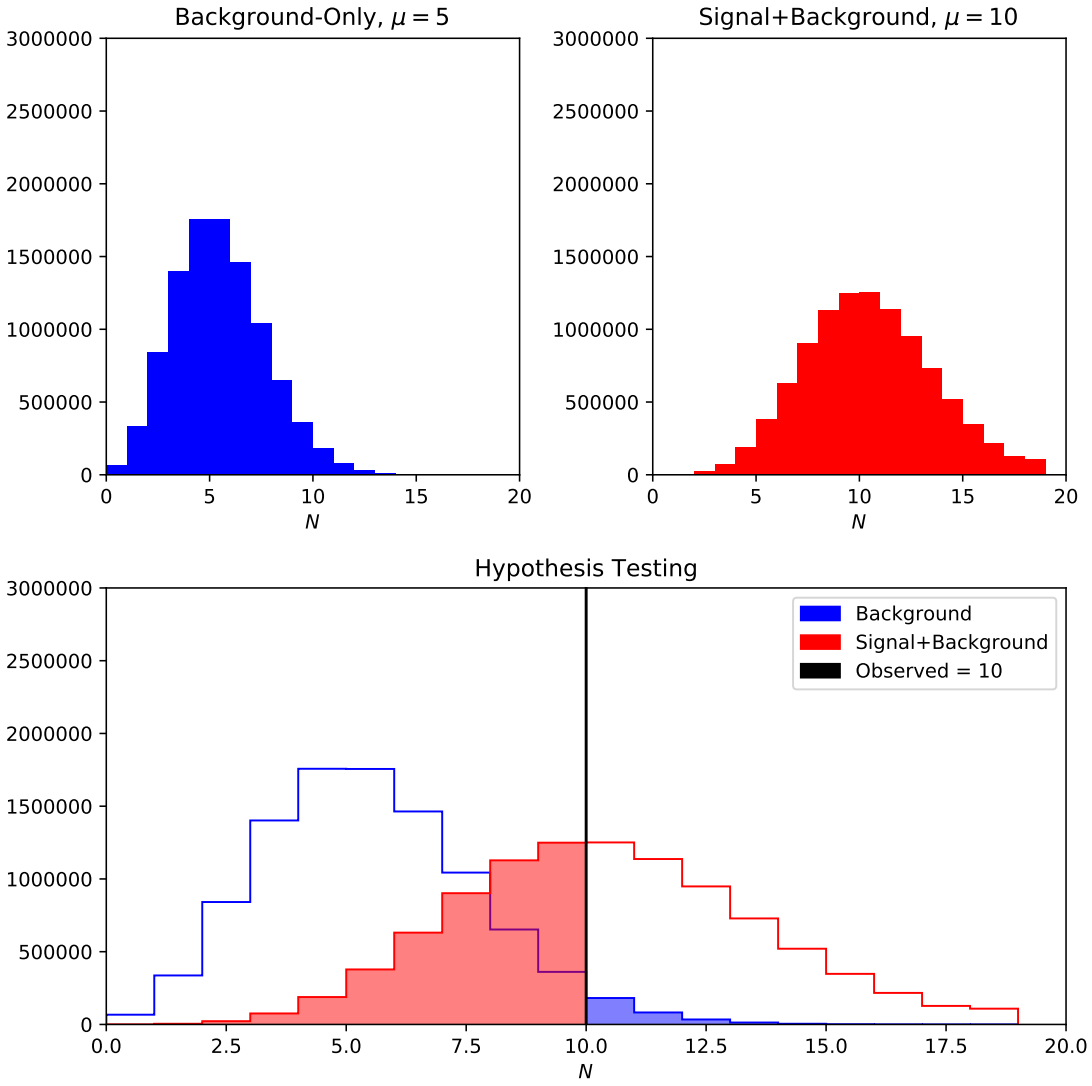

Figure 8.3: Example Poissonian probability density functions for background (blue) and signal+background (red) hypotheses for 10 observed events (black line). In this example, $p(10|b) = 0.018$ and $p(10|s+b) = 0.125$. The observed data is more likely under the $s+b$ hypothesis than background-only.

Note that the Neyman construction of parameter estimation can be rather cumbersome. There are two observables, n and b, and two possible true values, $s\mu, \hat{b}$. For each μ, the maximimum likelihood estimator of $\boldsymbol{\theta}$ is found, $\hat{\hat{\boldsymbol{\theta}}}(s\mu, n)$. However, as this procedure is remarkably computationally intensive, an approximation can be done by fixing $\hat{\hat{\boldsymbol{\theta}}}(s\mu, n_{\text{obs}})$ to reduce the dimensionality. Another useful feature of eq. (8.9) is that in the limit of large N (asymptotic or Asimov approximation), this can be evaluated analytically [6]. If this wasn't the case, this sort of determination would be computationally unfeasible due to the large number of systematics and signal model variables one needs to evaluate. Within ATLAS, it is convention to use the 95% CL, so that we exclude signal models with $\text{CL}_s < \alpha = 0.05$. For each the signal model being considered (**??**) and as described in **??**, each signal point is parameterized by the mass of the gluino, $\tilde{g}$, and the lightest supersymmetric particle, $\tilde{\chi}_1^0$. For each signal point, an exclusion fit is performed and the CL_s is calculated. Those with $\text{CL}_s < 0.05$ are excluded at the 95% CL. The last point of contention is to statisically combine the 0-lepton and 1-lepton regions to maximize the sensitivity. Each signal point will have six regions of CL_s computed, three for 0-lepton (boosted, moderate, compressed) and three for 1-lepton. For each region, model-dependent limits have been drawn and are shown in **??**. The signal region that provides the smallest CL_s at each signal point is chosen and collected into a "Gtt combination" plot shown in fig. 8.4. The $\pm 1\sigma_{\text{theory}}^{\text{SUSY}}$ lines around the observed limits are obtained by changing the SUSY cross-section by one standard deviation. The yellow band around the expected limit shows the $\pm 1\sigma$ uncertainty, including all statistical and systematic uncertainties expect the theoretical uncertainties in the SUSY cross-section. Compared to the previous results [9], the gluino mass sensitivies of the current search (assuming massless $\tilde{\chi}_1^0$) has improved by 450 GeV. Gluinos with masses below 1.97 TeV are excluded at the 95% CL for $\tilde{\chi}_1^0$ masses below 300 GeV.

The simplified model does make some explicit assumptions that may end up not being physical, however it is useful to frame the results of the search and its exclusion limits in the

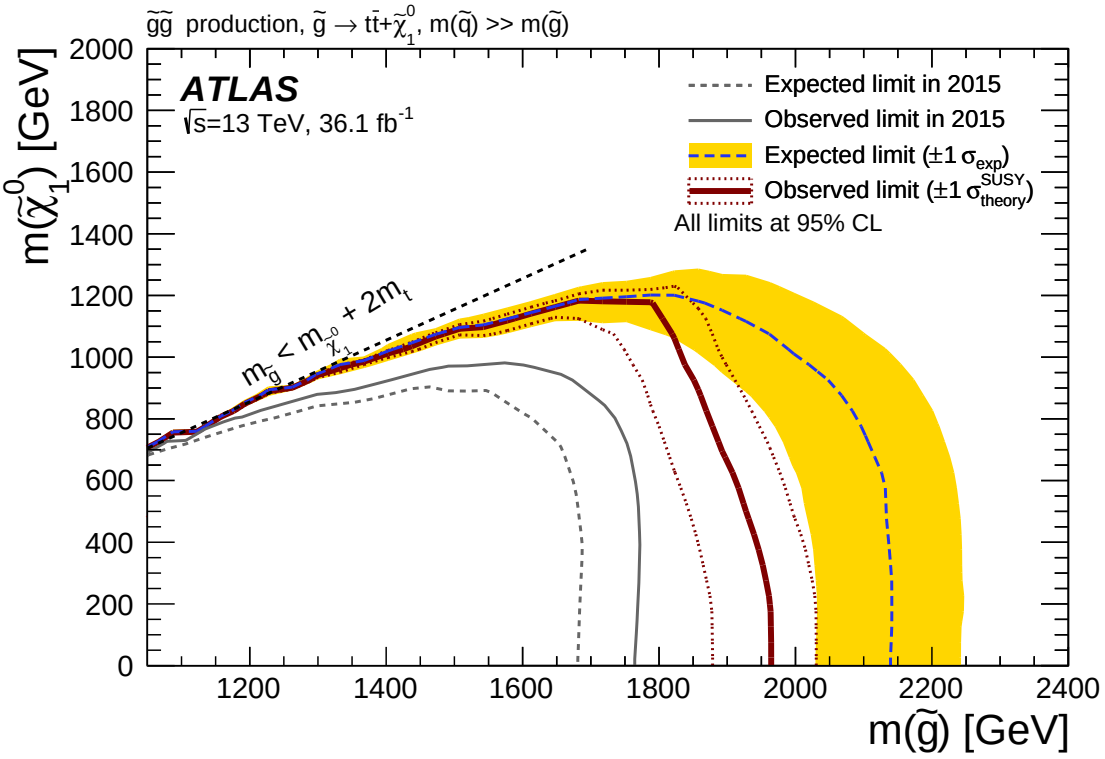

Figure 8.4: Exclusion limits in the $\tilde{\chi}_1^0$ and $\tilde{g}$ mass plane for the Gtt model obtained in the context of the cut-and-count analysis. The dashed and solid bold lines show the 95% CL expected and observed limits, respectively. The shaded bands around the expected limits show the impact of the experimental and background uncertainties. The dotted lines show the impact on the observed limit of the variation of the nominal signal cross-section by $\pm 1\sigma$ of its theoretical uncertainty. The 95% CL expected and observed limits from the ATLAS search based on 2015 data [9] are also shown.

context of other searches performed in fig. 8.5 for both the ATLAS and CMS collaborations that set limits in the $(\tilde{g}, \tilde{\chi}_1^0)$ mass plane. The results of the search described in this analysis is shown in magenta for the ATLAS summary plot.

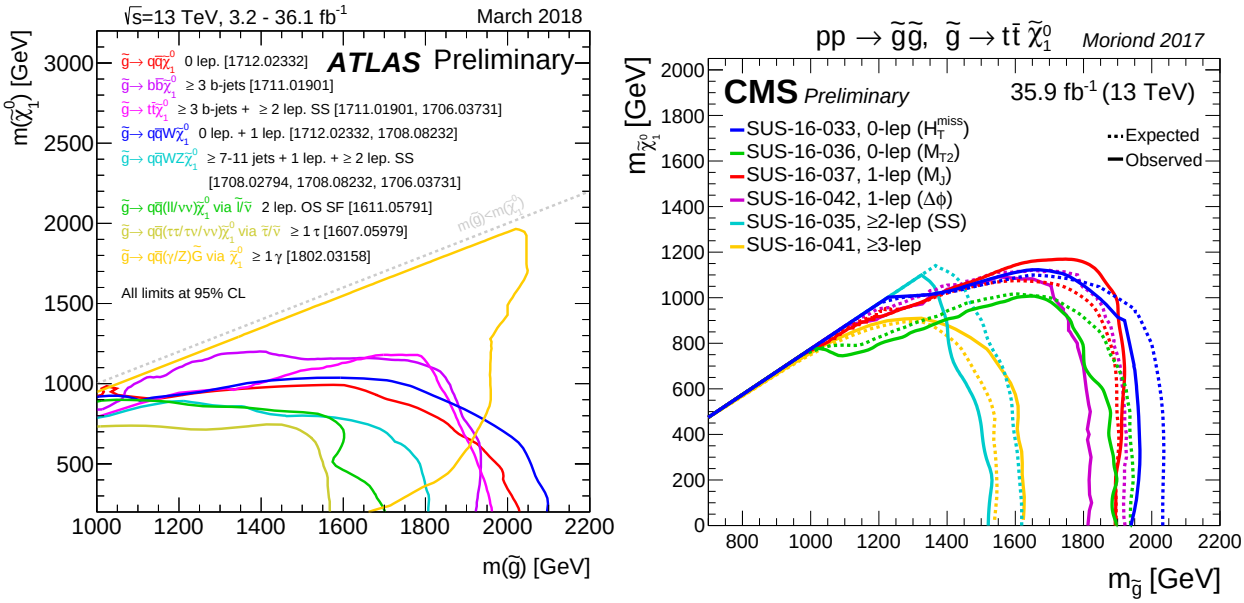

(a) [10] ATLAS

(b) [11] CMS

Figure 8.5: [10, 11] Exclusion limits at 95% CL based on 13 TeV data for (a) ATLAS and (b) CMS in the $(\tilde{g}, \tilde{\chi}_1^0)$ mass plane for different simplified models featuring the decay of the gluino to the lightest supersymmetric particle (lightest neutralino or gravitino) either directly or through a cascade chain featuring other SUSY particles with intermediate measses. For each line, the gluino decay mode is reported in the legend, along with the arXiv reference, and it is assumed to proceed with 100% branching ratio. Some limits depend on additional assumptions on the mass of the intermediate states, as described in the references provided in the plot (ATLAS [12, 4, 13, 14, 15, 16, 17]; CMS [18, 19, 20, 21, 22, 23]). The search presented in this thesis is shown in magenta for ATLAS.

8.4 Signal Acceptances and Experimental Efficiencies

These last set of plots I have made for HEPData [24] which allows for theorists and reinterpretation of existing searches by including measurements, cutflows, and efficiencies for the selections in an analysis. Two such examples of this data are the reconstruction efficiencies

and the detector acceptance of the signal models that we considered for this analysis. At a truth level, the signal acceptance provides a way to quantify what portion of the signal one can measure with a perfect detector for our selections, which is evaluated at a truth level using truth information in monte-carlo simulations. At a reconstruction level, the efficiency, really a detector acceptance $\otimes$ selection efficiency, quantifies the impact of the detector and our selections on the signal efficiency. So by evaluating these two forms, one can calculate the signal acceptance (truth), signal acceptance $\otimes$ efficiency (reconstruction), and divide the two to get a signal efficiency (incorporation reconstruction and truth) which quantifies the impact of the detector on our signal models. Figure 8.6 shows the three different plots for the 0-lepton boosted signal region selection. As seen towards the bottom right of the signal efficiency, the boosted regime suffers from a lower detector efficiency than in a more resolved region, motivating the need for detector-level improvements for boosted objects, such as the gFEX trigger upgrade I work on. See **??** for the full set of plots.

One potential complication is the fluctuations that are present because the analysis imposes very tight selections which can cause signal efficiencies $> 100\%$. For example, the b-tagging algorithm described in **??** does mis-tag light jets and c-jets as b-jets, but at a very reduced rate. Because our analysis requires at least three b-jets and the tight selections push it into extreme regions of the phase-space, the impact of mis-tagged jets is more amplified. In this case, the mis-tagging at the reconstruction level will artificially inflate the acceptance $\otimes$ efficiency compared to the truth level, where there is no mis-tagging. Dividing the truth level from the reconstruction level to get a signal efficiency can create an efficiency $> 100\%$.

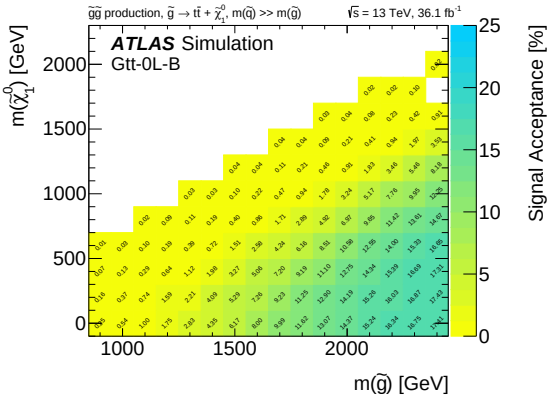

(a) Acceptance

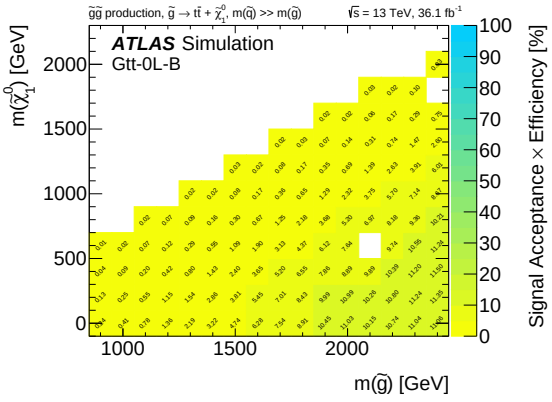

(b) Acceptance ⊗ Efficiency

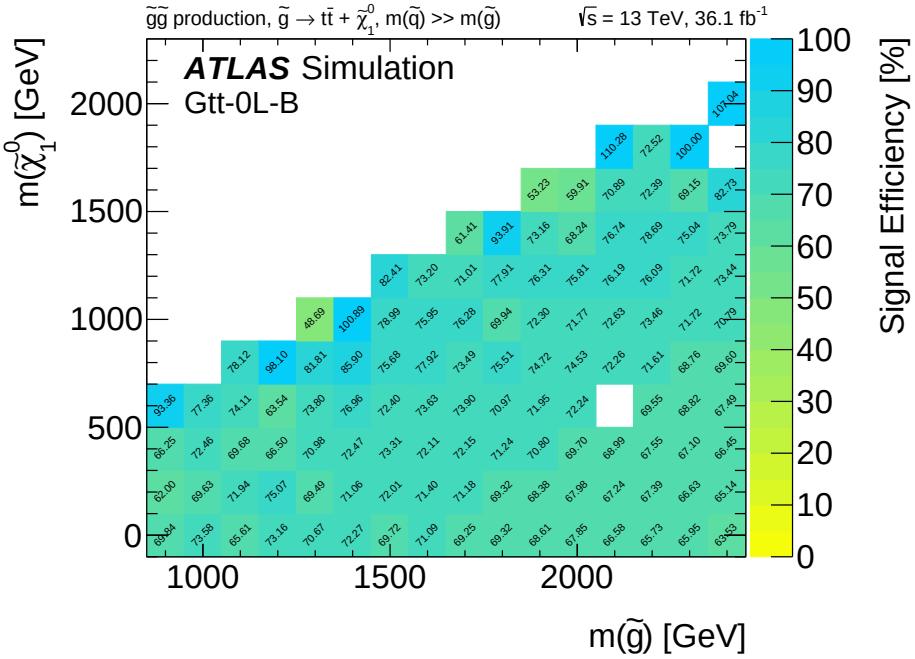

(c) Efficiency

Figure 8.6: For the Gtt 0-lepton boosted region, (a) signal acceptance at truth level, (b) signal acceptance ⊗ efficiency at the reconstruction level, and (c) calculated signal efficiency are shown in the ($\tilde{g}$, $\tilde{\chi}_1^0$) mass plane. The z-axis represents the value of each bin in units % with 0% being yellow, and 100% (25% for acceptance) being green.

Glossary

CL Confidence Level. 6, 10, 12–14

gFEX global Feature EXtractor.

SUSY Supersymmetry. 2

Bibliography

[1] M. Baak et al. "HistFitter software framework for statistical data analysis". In: *Eur. Phys. J. C* 75 (2015), p. 153. DOI: 10.1140/epjc/s10052-015-3327-7. arXiv: 1410.1280 [hep-ex] (cit. on pp. 2, 4).

[2] Kyle Cranmer et al. "HistFactory: A tool for creating statistical models for use with RooFit and RooStats". In: (2012) (cit. on pp. 2, 3).

[3] Kyle Cranmer and Itay Yavin. "RECAST: Extending the Impact of Existing Analyses". In: *JHEP 1104:038,2011* 04 (2010), p. 038. DOI: 10.1007/JHEP04(2011)038. arXiv: 1010.2506 [hep-ex] (cit. on p. 4).

[4] ATLAS Collaboration. "Search for Supersymmetry in final states with missing transverse momentum and multiple b-jets in proton–proton collisions at $\sqrt{s} = 13$ TeV with the ATLAS detector". In: (2017). arXiv: 1711.01901 [hep-ex] (cit. on pp. 6, 14).

[5] Michal Czakon and Alexander Mitov. "Top++: A Program for the Calculation of the Top-Pair Cross-Section at Hadron Colliders". In: *Comput. Phys. Commun.* 185 (2014), p. 2930. DOI: 10.1016/j.cpc.2014.06.021. arXiv: 1112.5675 [hep-ph] (cit. on p. 8).

[6] Glen Cowan et al. "Asymptotic formulae for likelihood-based tests of new physics". In: *Eur. Phys. J. C* 71 (2011), p. 1554. DOI: 10.1140/epjc/s10052-011-1554-0. arXiv: 1007.1727 [physics.data-an]. Erratum: Eur. Phys. J. C **73** (2013) 2501 (cit. on pp. 6, 12).

[7] Alexander L. Read. "Presentation of Search Results: The CL(s) Technique". In: *J. Phys. G* 28 (2002), p. 2693. DOI: 10.1088/0954-3899/28/10/313 (cit. on pp. 9, 10).

[8] and. "IX. On the problem of the most efficient tests of statistical hypotheses". In: *Philosophical Transactions of the Royal Society of London A: Mathematical, Physical and Engineering Sciences* 231.694-706 (1933), pp. 289–337. ISSN: 0264-3952. DOI: 10.1098/

rsta.1933.0009. eprint: http://rsta.royalsocietypublishing.org/content/231/694-706/289.full.pdf. URL: http://rsta.royalsocietypublishing.org/content/231/694-706/289 (cit. on pp. 9, 10).

[9] ATLAS Collaboration. "Search for pair production of gluinos decaying via stop and sbottom in events with b-jets and large missing transverse momentum in pp collisions at $\sqrt{s} = 13$ TeV with the ATLAS detector". In: *Phys. Rev. D* 94.3 (2016), p. 032003. DOI: 10.1103/PhysRevD.94.032003. arXiv: 1605.09318 [hep-ex] (cit. on pp. 12, 13).

[10] ATLAS Collaboration. *Summary plots from the ATLAS Supersymmetry physics group*. https://twiki.cern.ch/twiki/bin/view/AtlasPublic/SupersymmetryPublicResults. [Online; accessed 08-April-2018]. 2015 (cit. on p. 14).

[11] CMS Collaboration. *Summary plots from the CMS Supersymmetry physics group*. https://twiki.cern.ch/twiki/bin/view/CMSPublic/PhysicsResultsSUS. [Online; accessed 08-April-2018]. 2015 (cit. on p. 14).

[12] Morad Aaboud et al. "Search for squarks and gluinos in final states with jets and missing transverse momentum using 36 fb^{-1} of $\sqrt{s}$=13 TeV pp collision data with the ATLAS detector". In: (2017). arXiv: 1712.02332 [hep-ex] (cit. on p. 14).

[13] Morad Aaboud et al. "Search for supersymmetry in final states with two same-sign or three leptons and jets using 36 fb^{-1} of $\sqrt{s} = 13$ TeV pp collision data with the ATLAS detector". In: *JHEP* 09 (2017), p. 084. DOI: 10.1007/JHEP09(2017)084. arXiv: 1706.03731 [hep-ex] (cit. on p. 14).

[14] Morad Aaboud et al. "Search for squarks and gluinos in events with an isolated lepton, jets, and missing transverse momentum at $\sqrt{s} = 13$ TeV with the ATLAS detector". In: *Phys. Rev.* D96.11 (2017), p. 112010. DOI: 10.1103/PhysRevD.96.112010. arXiv: 1708.08232 [hep-ex] (cit. on p. 14).

[15] Morad Aaboud et al. "Search for new phenomena in events containing a same-flavour opposite-sign dilepton pair, jets, and large missing transverse momentum in $\sqrt{s} = 13$ pp collisions with the ATLAS detector". In: *Eur. Phys. J.* C77.3 (2017), p. 144. DOI: 10.1140/epjc/s10052-017-4700-5. arXiv: 1611.05791 [hep-ex] (cit. on p. 14).

[16] Morad Aaboud et al. "Search for squarks and gluinos in events with hadronically decaying tau leptons, jets and missing transverse momentum in proton-proton collisions at $\sqrt{s} = 13$ TeV recorded with the ATLAS detector". In: *Eur. Phys. J.* C76.12 (2016), p. 683. DOI: 10.1140/epjc/s10052-016-4481-2. arXiv: 1607.05979 [hep-ex] (cit. on p. 14).

[17] Morad Aaboud et al. "Search for photonic signatures of gauge-mediated supersymmetry in 13 TeV pp collisions with the ATLAS detector". In: (2018). arXiv: 1802.03158 [hep-ex] (cit. on p. 14).

[18] CMS Collaboration. "Search for supersymmetry in multijet events with missing transverse momentum in proton–proton collisions at 13 TeV". In: *Phys. Rev. D* 96 (2017), p. 032003. DOI: 10.1103/PhysRevD.96.032003. arXiv: 1704.07781 [hep-ex] (cit. on p. 14).

[19] CMS Collaboration. "Search for new phenomena with the M_{T2} variable in the all-hadronic final state produced in proton–proton collisions at $\sqrt{s} = 13$ TeV". In: (2017). arXiv: 1705.04650 [hep-ex] (cit. on p. 14).

[20] CMS Collaboration. "Search for supersymmetry in pp collisions at $\sqrt{s} = 13$ TeV in the single-lepton final state using the sum of masses of large-radius jets". In: *Phys. Rev. Lett.* 119 (2017), p. 151802. DOI: 10.1103/PhysRevLett.119.151802. arXiv: 1705.04673 [hep-ex] (cit. on p. 14).

[21] CMS Collaboration. "Search for supersymmetry in events with one lepton and multiple jets exploiting the angular correlation between the lepton and the missing transverse

momentum in proton–proton collisions at $\sqrt{s} = 13$ TeV". In: (2017). arXiv: 1709.09814 [hep-ex] (cit. on p. 14).

[22] CMS Collaboration. "Search for physics beyond the standard model in events with two leptons of same sign, missing transverse momentum, and jets in proton–proton collisions at $\sqrt{s} = 13$ TeV". In: *Eur. Phys. J. C* 77 (2017), p. 578. DOI: 10.1140/epjc/s10052-017-5079-z. arXiv: 1704.07323 [hep-ex] (cit. on p. 14).

[23] CMS Collaboration. "Search for supersymmetry in events with at least three electrons or muons, jets, and missing transverse momentum in proton–proton collisions at $\sqrt{s} =$ 13 TeV". In: (2017). arXiv: 1710.09154 [hep-ex] (cit. on p. 14).

[24] Eamonn Maguire, Lukas Heinrich, and Graeme Watt. "HEPData: a repository for high energy physics data". In: *J. Phys. Conf. Ser.* 898.10 (2017), p. 102006. DOI: 10.1088/1742-6596/898/10/102006. arXiv: 1704.05473 [hep-ex] (cit. on p. 14).